Journal of Visualized Experiments

# Confocal laser scanning microscopy-based quantitative analysis of A. fumigatus conidia distribution in whole-mount optically cleared mouse lung

--Manuscript Draft--

| | |
|---|---|
| **Article Type:** | Invited Methods Collection - Author Produced Video |
| **Manuscript Number:** | JoVE62436R5 |
| **Full Title:** | Confocal laser scanning microscopy-based quantitative analysis of A. fumigatus conidia distribution in whole-mount optically cleared mouse lung |
| **Corresponding Author:** | Marina Shevchenko<br>Shemyakin-Ovchinnikov Institute of Bioorganic Chemistry Russian Academy of Sciences: FBGUN Institut bioorganiceskoj himii im akademikov M M Semakina i U A Ovcinnikova Rossijskoj akademii nauk<br>Moscow, RUSSIAN FEDERATION |
| **Corresponding Author's Institution:** | Shemyakin-Ovchinnikov Institute of Bioorganic Chemistry Russian Academy of Sciences: FBGUN Institut bioorganiceskoj himii im akademikov M M Semakina i U A Ovcinnikova Rossijskoj akademii nauk |
| **Corresponding Author E-Mail:** | mshevch@gmail.com |
| **Order of Authors:** | Ivan Maslov |
| | Andrey Bogorodskiy |
| | Mariia Pavelchenko |
| | Ilia Zykov |
| | Natalya Troyanova |
| | Valentin Borshchevskiy |
| | Marina Shevchenko |
| **Additional Information:** | |
| **Question** | **Response** |
| Please indicate whether this article will be Standard Access or Open Access. | Standard Access (US$1200) |
| Please specify the section of the submitted manuscript. | Immunology and Infection |
| Please confirm that you have read and agree to the terms and conditions of the author license agreement that applies below: | I agree to the Author License Agreement |
| Please provide any comments to the journal here. | |
| Please indicate whether this article will be Standard Access or Open Access. | Standard Access ($1400) |
| Please confirm that you have read and agree to the terms and conditions of the video release that applies below: | I agree to the Video Release |

**TITLE:**

# Confocal Laser Scanning Microscopy-Based Quantitative Analysis of *Aspergillus fumigatus* Conidia Distribution in Whole-Mount Optically Cleared Mouse Lung

**AUTHORS AND AFFILIATIONS:**

Ivan V Maslov[1], Andrey O Bogorodskiy[1], Mariia V Pavelchenko[1], Ilia O Zykov[1], Natalya I Troyanova[2], Valentin V Borshchevskiy[3,1]*, Marina A Shevchenko[2]*

[1]Research Center for Molecular Mechanisms of Aging and Age-Related Diseases, Moscow Institute of Physics and Technology, Dolgoprudny, Russia

[2]Department of Immunology, Shemyakn and Ovchinnikov Institute of Bioorganic Chemistry, Russian Academy of Sciences, Moscow, Russia

[3]Institute of Biological Information Processing (IBI-7: Structural Biochemistry), Forschungszentrum Jülich, Jülich, Germany

Corresponding Authors:
Marina A Shevchenko
shev@ibch.ru (or mshevch@gmail.com)
&
Valentin I Borshchevskiy
borshchevskiy.vi@phystech.edu

Email Addresses of Co-authors**:**
Andrey O Bogorodskiy (bogorodskiy173@gmail.com)
Mariia V Pavelchenko (mariya.pavelchenko@phystech.edu)
Ilia O Zykov (ilya.o-zykov@yandex.ru)
Ivan V Maslov (ivan.v.maslov@phystech.edu)
Natalya I Troyanova (troyanatali@gmail.com)

**KEYWORDS:**

*Aspergillus fumigatus*, conidia distribution, optically cleared mouse lung, fluorescent confocal laser scanning microscopy

**SUMMARY:**

We describe the method for quantitative analysis of the distribution of *Aspergillus fumigatus* conidia (3 µm in size) in the airways of mice. The method also can be used for the analysis of microparticles and nanoparticle agglomerate distribution in the airways in various pathological condition models.

**ABSTRACT:**

*Aspergillus fumigatus* conidia are airborne pathogens that can penetrate human airways. Immunocompetent people without allergies exhibit resistance and immunological tolerance, while in immunocompromised patients, conidia can colonize airways and cause severe invasive respiratory disorders. Various cells in different airway compartments are involved in the immune

response that prevents fungal invasion; however, the spatio-temporal aspects of pathogen elimination are still not completely understood. Three-dimensional (3D) imaging of optically cleared whole-mount organs, particularly the lungs of experimental mice, permits detection of fluorescently labeled pathogens in the airways at different time points after infection. In the present study, we describe an experimental setup to perform a quantitative analysis of *A. fumigatus* conidia distribution in the airways. Using fluorescent confocal laser scanning microscopy (CLSM), we traced the location of fluorescently labeled conidia in the bronchial branches and the alveolar compartment 6 hours after oropharyngeal application to mice. The approach described here was previously used for detection of the precise pathogen location and identification of the pathogen-interacting cells at different phases of the immune response. The experimental setup can be used to estimate the kinetics of the pathogen elimination in different pathological conditions.

**INTRODUCTION:**

On a daily basis, people inhale airborne pathogens, including spores of opportunistic fungi *Aspergillus fumigatus* (*A. fumigatus* conidia) that can penetrate the respiratory tract[1]. The respiratory tract of mammals is a system of airways of different generations that are characterized by the different structures of the airway walls[2,3,4]. Tracheobronchial walls consist of several cell types among which are ciliated cells that provide the mucociliary clearance[5]. In the alveoli, there are no ciliated cells and the penetrating alveolar space pathogens cannot be eliminated by the mucociliary clearance[6]. Moreover, each airway generation is a niche for multiple immune cell populations and subsets of these populations are unique for certain airway compartments. Thus, alveolar macrophages reside in the alveolar compartments, while both the trachea and conducting airways are lined with the intraepithelial dendritic cells[7,8].

The approximate size of *A. fumigatus* conidia is 2-3.5 µm[9]. Since the diameter of small airways in humans and even in mice exceeds 3.5 µm, it was suggested that conidia can penetrate the alveolar space[2,10,11]. In fact, histological examination showed the fungal growth in the alveoli of the patients suffering from aspergillosis[12]. Conidia were also detected in the alveoli of infected mice using live imaging of the thick lung slices[13]. Simultaneously, conidia were detected in the luminal side of the bronchial epithelium of mice[14].

Three-dimensional (3D) imaging of the optically cleared whole-mount mouse lungs permits morphometric analysis of the airways[15]. Particularly, the quantitative analysis of the visceral pleural nerve distribution was performed using optically cleared mouse lung specimens[15]. Recently, Amich et al.[16] investigated the fungal growth after intranasal application of conidia to the immunocompromised mice using a light-sheet fluorescence microscopy of optically cleared mouse lung specimens. The precise location of the resting conidia in the airways at different time points after the infection is important for identifying the cell populations that can provide sufficient antifungal defense in certain phases of inflammation. However, due to the relatively small size, the spatio-temporal aspects of *A. fumigatus* conidia distribution in the airways are poorly characterized.

Here, we present an experimental setup for the quantitative analysis of *A. fumigatus* conidia

distribution in the airways of infected mice. Using fluorescent confocal laser scanning microscopy (CLSM) of optically cleared lungs of mice that received an oropharyngeal application of the fluorescently labeled *A. fumigatus* conidia, we obtain 3D images and perform the image processing. Using 3D imaging of the whole-mount lung lobe, we have previously shown the distribution of *A. fumigatus* conidia in the conducting airway of mice 72 hours after conidia application[8].

**PROTOCOL:**

All methods concerning laboratory animals described here have been approved by the Institutional Animal Care and Use Committee (IACUC) at the Shemyakin and Ovchinnikov Institute of Bioorganic Chemistry, Russian Academy of Sciences (protocol number 226/2017).

## 1. *A. fumigatus* conidia application

1.1 To obtain fluorescently labeled *A. fumigatus* conidia, fix $5 \times 10^8$ conidia by adding 1 mL of 3% paraformaldehyde to the conidia pellet. Incubate in a 50 mL test tube for 2 h on a shaker at room temperature.

1.2 Wash conidia with 20 mL of phosphate buffer saline (PBS) by centrifuging at 1,000 x g for 15 min, gently removing the supernatant, and adding fresh PBS in a volume of 20 mL. Repeat.

1.3 Dissolve the conidia in 900 µL of 0.1 M $NaHCO_3$.

1.4 Dissolve the succinimidyl ester of the 594-fluorescent dye in 100 µL of dimethyl sulfoxide and add to conidia.

1.5 Incubate the conidia with the dye for 1 h on a shaker at 150 rpm at room temperature.

1.6 Wash the conidia twice with 20 mL of PBS in the centrifuge at 1,000 x g for 15 min.

1.7 Dilute the conidia to a concentration of $1 \times 10^8$ conidia/mL in PBS and store at 4 °C.

1.8 Anesthetize the mouse with 0.5-3% isoflurane vapor. Put the mouse on the holder, fix the tongue with smooth forceps, and hold the nares. Take a single channel pipette and apply 50 µL of conidia suspension to the mouse pharynx. Wait until the suspension is inhaled.

## 2. Specimen preparation

2.1 Prepare the 50 mL test tube and fill it with 15 mL of fresh 2% paraformaldehyde. Place the medical instruments (15 cm toothed dissecting forceps, 8 cm fine-tipped forceps, and 10 cm scissors with blunt ends) into 70% ethanol solution.

2.2 Euthanize the mouse in accordance with the IACUC protocol euthanized. Then place the mouse in the dorsal position and fix the mouse paws with needles.

NOTE: If using cervical dislocation for euthanasia, ensure the integrity of the trachea.

2.2.1 Treat the mouse with 70% ethanol using a sprayer.

2.2.2 Make a median longitudinal cut in the ventral skin from the hind paws to the forepaws and the chin.

2.2.3 Separate the skin from the subcutaneous tissue using toothed forceps and closed scissors. Fix the upper ends of the skin with needles.

2.2.4 Make an incision in the abdominal wall and separate the liver from the diaphragm. Carefully pick the diaphragm with closed scissors and then cut the diaphragm.

2.2.5 Make a medial cut of the thorax and neck connective tissues until the trachea is visible.

2.3 Run a silk thread beneath the trachea and make a surgical knot using two forceps.

NOTE: Alternatively, use dental floss instead of silk thread.

2.3.1 Carefully pull the thread and cut off the lungs from the connective tissue with scissors. Hold the scissors perpendicular to the table.

2.3.2 Put the lungs in the 50 mL test tube with 2% paraformaldehyde. Leave thread ends outside the tube, put the cover tight, and turn over the tube to cover the lungs with paraformaldehyde. Hold the lungs overnight at 4 °C.

2.4 Dissect the lung lobes from the heart and each other with a scalpel.

2.4.1 Put the lung lobes in a 24 well plate, with each lobe in a separate well. Wash the lung lobes in 1 mL of Tris-buffered saline (TBS) pH 7.4, 5 times for 1 h each on a shaker at 150 rpm.

2.4.2 Replace 1 mL of TBS with 1 mL of the blocking buffer (1% Triton X 100, 5% powdered milk in TBS) and leave the specimen overnight at room temperature on a shaker.

2.4.3 Replace the blocking buffer with 1 mL of streptavidin-488-fluorescent dye conjugate diluted 1:30 in TBS. Leave the specimen for at least 72 h at room temperature on a shaker (150 rpm).

2.5 Wash the specimen 5 times for 1 h each in 1 mL of TBS at room temperature on a shaker (150 rpm). Transfer the specimen to the new wells and cover it with 2% paraformaldehyde overnight at 4 °C for post-fixation.

## 3. Mouse lung lobe optical clearing

3.1. Place the specimen in the 5 mL glass bottle filled with 3 mL of 50% methanol-water solution and put it on to the sample mixer at room temperature for 1 h.

3.2. Replace 3 mL of 50% methanol with 3 mL of 100% methanol and put it on to the sample mixer for 2 h. Prepare a 1:2 v/v mixture of benzyl alcohol and benzyl benzoate (BABB) in a total volume of 1 mL.

3.3. Transfer the specimen to a 24 well plate and cover with 1 mL of BABB mixture for at least 30 min. Do not leave the specimen in BABB for a long time; BABB can damage the plastic plate and make the specimen too rigid.

3.4. Put the specimen in the cell imaging coverglass-bottom chamber. The sample is ready for imaging.

## 4. Mouse lung lobe imaging with CLSM

4.1. Turn the microscope system on. Open the microscope software. Turn the transmission light on in the **Locate** tab. Select the 10x objective.

NOTE: For more detailed analysis, use the 20x objective, but it increases the time of the experiment and the image file size.

4.2. Put the chamber with the specimen in the cover slide holder. Put the holder on the XY stage over the objective. Center the specimen using the XY controls of the stage on top of the objective. Use the transmission light and eyepiece to manually find the specimen Z-plane.

4.3. Switch the software to the **Acquisition** tab. Select **CLSM λ**-mode. Turn the 488 nm and 561 nm lasers on. Select the 488/561 nm dichroic mirror. Change the spectral range of the detector to 490-695 nm. Adjust the laser power to the appropriate range (10-50 µW). Adjust the **Detector Gain** between 750-900 range.

NOTE: Higher gain settings are undesirable due to noise.

4.4. Narrow the pinhole to 1 Airy unit by clicking **1 AU** button. Set pixel resolution to **512 × 512** pixels.

4.5. Switch on the **Z-stack** mode. Start **Live Imaging**. Select the focal plane in which both dyes are visible.

NOTE: If necessary, adjust the laser power to normalize the brightness of the two fluorescent dyes. Use **Gallery** and **Single-channel** mode, to avoid clipping and to precisely match fluorescence intensity.

4.6. Expand the appeared **Z-stack** pane. Use the focusing wheel and find the lowest plane of the sample. Use the **First** button in the **Z-stack** pane. Move the focal plane upwards to find the top boundary of the specimen and save the position by using the **Last** button. Check the representation of the sample depth in the **Z-stack** pane.

NOTE: A representation of the sample depth will appear in the **Z-stack** pane after the **First** and the **Last** positions are chosen.

4.7. Position the objective using the focusing wheel near the bottom of the specimen, by looking at the **Z-stack** pane. This is approximately 20 µm from the bottom of the specimen.

4.8. Turn the **Z-stack** mode off and turn the **Tile Scan** mode on. Acquire the image with an appropriate number of tiles for the size of the specimen. 5 × 5 tiles are a good starting point.

4.9. Adjust the number of tiles and the specimen XY position until the whole lung fits inside the tiled image. Recheck the correctness of the **Z-stack** positions with the newly obtained XY position of the center of the sample.

4.10. Turn both **Z-stack** and **Tile Scan** modes on. Set Z step (in **Z-stack** pane) to 5 µm. Set **Scanning Speed** to 6. Turn the **Autosave** function on. Turn the option **Saving Separate Tiles** on. Name the file. Press the **Start Experiment** button.

4.11. Verify that the experiment does not exceed the allocated time on the microscope; if so – adjust the speed.

NOTE: The approximate file size is more than 10 Gb; be sure that there is enough space on the hard drive.

## 5. Spectral unmixing and stitching

5.1. Use the software for the initial image processing. For spectral unmixing, select the **Unmixing** option. Select two regions corresponding to the streptavidin/airways and conidia to acquire the spectra from the image. Click **Start Unmixing**.

NOTE: Alternatively, use the existing spectra for 488 and 594 nm fluorochromes.

5.2. Open the file for the image processing and select the **Processing** tab. In the **Methods** section, select **Geometric** and **Stitching**. In the **Parameter** section, select the **New Output** and mark the **Fuse Tiles** option. Use the reference mode with the selected channel corresponding to the airway fluorescence. Apply the Stitching by clicking **Apply**.

## 6. Image processing: surface rendering

6.1. Open the image as a **Surpass 3D View**. Create an airway surface using the option **Surface** for the channel that was used for the airway visualization. Choose the **Smoothing** parameter of 10 µm.

NOTE: Choose the automatic threshold value as well.

6.2. Visually inspect the surface. Choose the thresholds to reduce the outlying signal. Remove the surfaces of pleura and vessels.

6.3. Create a mask for the airway surface using options **Edit** and **Mask All**. Select the airway channel and set **Voxels outside the surface** to 0.001.

6.4. Save the file with the airway mask as a TIFF series to the folder. Save the file with the conidia channel as a TIFF series to the separate folder.

## 7. Image processing: mask correction

7.1. Open the file with the airway mask in an open-source platform for biological-image analysis[17] as an 8-bit image. Make the image binary by clicking **Process** | **Binary** | **Make Binary**.

NOTE: If necessary, correct the mask: remove the excessive surfaces using the **Polygon selection** and **Delete** tab. Alternatively, use the **Flood Fill Tool**.

7.2. Draw the missing surfaces using several times **Dilate (3D)**: click **Plugins** | **Process** | **Dilate (3D).** Fill the holes by clicking **Process** | **Binary** | **Fill Holes**. Use selection and **ROI manager interpolation** to fill the residual holes in the mask manually. Apply several **Erode (3D)** options (**Plugins** | **Process** | **Erode (3D)**) to resample the mask thickness.

NOTE: Create macros by using **Plugins** | **Macros** options for multiple **Dilate (3D)** and **Erode (3D)** repeats.

Ensure the number of **Erode (3D)** is equal to the number of **Dilate (3D)** applications.

7.3. Save the mask in a new folder as a TIFF series.

## 8. Conidia quantitative analysis

8.1. Open the app in the programming and numeric computing platform: https://www.mathworks.com/matlabcentral/fileexchange/84525-conidia_counter.

8.2. Press the **Add files** button. Select the airway mask folder and the conidia folder.

8.3. Set a **custom threshold** between 0 and 1. Press the **OK** button.

8.4. Save the output table to the custom .xls file.

8.5. Analyze the data with software for statistical analysis.

**REPRESENTATIVE RESULTS:**

Following the protocol above, the 3D image showing the airways and *A. fumigatus* conidia in the lung lobe of a mouse was obtained (**Figure 1A**). Streptavidin (that was used for airway visualization) labeled bronchi and bronchioles[15]. Additionally, the large vessels, which are easily distinguishable from the airways by their morphology, and pleura are visualized in the airway channel (**Figure 1A-C**). The creation of the airway surface and mask permitted removal of the vessel and the pleura projections in the airway channel; however, the integrity of the airway surface is destroyed due to the weak signal of streptavidin in several bronchial branches (**Figure 1B-C**). The further processing of the airway mask permits the repair of the missing fragments (**Figure 1D**).

The distribution of *A. fumigatus* conidia in the lungs of mice was estimated using the left or right superior lung lobes at different time points after conidia application. For the right superior lung lobe, the image consists of approximately 30 tiles and around 250 Z-stacks. After stitching, the image that was acquired with the resolution 512 × 512 had an image size of 2360 × 2815 pixels and the size of one pixel is 2.77 µm × 2.77 µm, which is comparable with the size of *A. fumigatus* conidia that is 2-3.5 µm[9].

The enlarged image of the distal airway region demonstrates that detection of the precise location of conidia (inside or outside the bronchial branches) is quite difficult due to the complexity of the image and the small size of conidia in relation to the size of the airways (**Figure 2A**). Precise examination revealed that conidia were located both inside and outside the bronchial branches (**Figure 2B-C**).

The threshold settings of the conidia channel greatly influence the resulting number of conidia (**Figure 2B-C**). To make the unbiased quantitative analysis we developed an app in the programming and numeric computing platform that allows estimating the number of conidia inside and outside the airway mask, avoiding the manual threshold setting. The app acts based on the following algorithm. First, the conidia channel is segmented into a binary 3D stack of images using an optimal threshold value. As was described above, the selected imaging resolution permits the identification of one conidium as one pixel. The usage of streptavidin for airway labeling permits visualization of bronchi but not alveoli[15]. Therefore, conidia residing in bronchi are defined as conidia pixels inside the airways mask, while conidia residing in alveoli are defined as conidia pixels outside the airway mask. Considering this, in the next step of the algorithm, a binary AND operation is performed for the airway mask image and the conidia image to extract pixels of conidia that reside in bronchi. Similarly, the remaining conidia pixels are extracted to obtain the number of conidia in alveoli. The resulting percentage of conidia in

bronchi and alveoli relative to the overall amount of conidia in the lung is presented in the bar chart and the output table of the app user interface.

Using this approach, the quantitative analysis of the conidia distribution in the airways of mice was performed for the time point of 6 hours after conidia application (**Figure 2D**). The data suggest that upon oropharyngeal application, the majority of conidia penetrate the alveolar space and locate there at the beginning of the inflammatory immune response.

**FIGURE AND TABLE LEGENDS:**

**Figure 1. The principle of airway image processing.** (**A**) 3D image of the right superior lung lobe of a mouse, 24 hours after conidia application showing biotin-rich structures (streptavidin, white) and *A. fumigatus* conidia (magenta). (**B,C**) The surface (green) and the mask (orange) for the airways. Streptavidin-positive large vessels are indicated with fine arrows. The missing airway fragments in the surface and the mask are indicated with arrows; the excessive structures with arrowheads. Scale bar is 1000 µm. (**D**) The airway mask after the corrections.

**Figure 2. Conidia image processing and quantitative analysis.** (**A**) Enlarged image of the distal airways (Streptavidin, grey shades) and *A. fumigatus* conidia (magenta) that are presented in **Figure 1A**. Scale bar is 300 µm **B, C**. Enlarged image arbitrary boxed on (**A**) is represented as a Z-slice with a high threshold (**B**) and a low threshold value (**C**). Conidia inside the airway are indicated with arrows, and outside with arrowheads. Scale bar is 150 µm. (**D**) Quantitative analysis of conidia in the bronchial branches and the alveolar space. The data are shown as the median and interquartile range for 4 mice, 6 h after receiving *A. fumigatus* conidia.

**DISCUSSION:**

Whole-organ 3D imaging permits obtaining of the data without dissection of the specimen, which is of great importance for investigating the spatial aspects of the anatomical distribution of the pathogen in the organism. There are several techniques and modifications of tissue optical clearing that help to overcome the laser light scattering and allow whole-organ imaging[15,16,18,19]. One of the custom tissue clearing approaches consists of methanol-based tissue dehydration and delipidation followed by optical clearing with BABB. The approach was developed more than 100 years ago and has several modifications. In our work, we use the simplest modification that was described by Scott *et al.*[15] Such an approach is optimal for usage with fluorescently labeled pathogens. Moreover, the fluorochromes with high photostability are preferable for prolonged imaging. Unfortunately, visualization of transgenic TdTomato *A. fumigatus* conidia is not possible using this method, due to the high sensitivity of TdTomato to BABB (data not shown). Thus, the approach that we describe here permits successful detection of resting or fixed pathogens, but cannot be used for imaging of growing *A. fumigatus* conidia or hyphae. Additionally, the immunohistochemical staining of the specimen with the high-affinity binding substances is preferable. Thus, we also faced trouble trying to apply the fluorescently labeled antibodies to visualize vessels and lymphatics in whole-mount lung lobe specimens. However, Scott *et al.*[15] visualized nerve fibers using two-step staining with antibodies against PGP 9.5. This indicates that some antibodies can be used for staining with the following optical clearing using BABB. We also lost the fluorescent signal from the 0.1 µm fluorescent latex particles after BABB clearing, while

the usage of clearing-enhanced 3D (Ce3D) clearing solution[18] did not affect the fluorescent signal of the particles.

In the present approach, we use streptavidin to label airways. Streptavidin binds endogenous biotin that is considered to be expressed in Clara cells (and the alveolar type II epithelial cells to a lesser extent)[20]. As Clara cells (also known as Club cells) in the absence of inflammation reside in the bronchi and bronchioles, but not in the alveolar compartment, streptavidin staining visualizes only bronchial branches. Therefore, in the present approach, all the conidia outside the streptavidin-labeled airways were determined as being located in the alveolar space. For the more precise detection of the conidia location, some other airway markers, such as SOX9, should be used[3]. In case, when antibody usage is necessary Ce3D or three-dimensional imaging of solvent-cleared organs (3DISCO)[19] techniques are more appropriate than BAAB-based optical clearing. However, BABB optical clearing is the most simple and time-consuming approach, and therefore is the most advantageous for the in advance fluorescently labeled conidia detection in the marked with streptavidin airways.

3D imaging of the mouse lungs can also be performed using optical projection tomography integrated microscopy[3]. However, due to the limitation in the resolution of tomography, CLSM is more suitable for the simultaneous imaging of the airways and 3 µm conidia. In our case, a single conidium is seen as one pixel. The processing of such images allowed quantification of conidia inside and outside the bronchial branches. The method also can be applied to compare anatomical conidia distribution in the immunocompetent and immunocompromised mice. The approach can also be utilized to estimate the kinetics of the conidia elimination from the airways of mice. Moreover, the combination of the approach of the whole airway morphometry that was developed by Scott *et al.*[15] with the algorithm for unbiased conidia quantitative analysis can be helpful in the precise location of *A. fumigatus* conidia and other particles of comparable size in different generations of the bronchial tree.

**ACKNOWLEDGMENTS:**

The authors thank Prof. Sven Krappmann (University Hospital Erlangen and FUA Erlangen-Nürnberg, Germany) for providing the *Aspergillus fumigatus* conidia strain AfS150. The authors thank MIPT Press Office. V.B. acknowledges the Ministry of Science and Higher Education of the Russian Federation (#075-00337-20-03, project FSMG-2020-0003). The work regarding *A. fumigatus* conidia imaging and quantification was supported by RSF № 19-75-00082. The work regarding airways imaging was supported by RFBR № 20-04-60311.

**DISCLOSURES:**

The authors report no conflicts of interest in this work.

**REFERENCES:**

1. O'Gorman, C.M. Airborne Aspergillus fumigatus conidia: A risk factor for aspergillosis. *Fungal Biology Reviews*. **25** (3), 151–157, doi: 10.1016/j.fbr.2011.07.002 (2011).
2. Hyde, D.M. *et al.* Asthma: A comparison of animal models using stereological methods. *European Respiratory Review*. **15** (101), 122–135, doi: 10.1183/09059180.00010103 (2006).

438 3. Alanis, D.M., Chang, D.R., Akiyama, H., Krasnow, M.A., Chen, J. Two nested developmental
439 waves demarcate a compartment boundary in the mouse lung. *Nature Communications*. **5**, doi:
440 10.1038/ncomms4923 (2014).
441 4. Kleinstreuer, C., Zhang, Z., Donohue, J.F. Targeted drug-aerosol delivery in the human
442 respiratory system. *Annual Review of Biomedical Engineering*. **10**, doi:
443 10.1146/annurev.bioeng.10.061807.160544 (2008).
444 5. Bustamante-Marin, X.M., Ostrowski, L.E. Cilia and mucociliary clearance. *Cold Spring*
445 *Harbor Perspectives in Biology*. **9** (4), doi: 10.1101/cshperspect.a028241 (2017).
446 6. Fröhlich, E., Salar-Behzadi, S. Toxicological assessment of inhaled nanoparticles: Role of
447 in vivo, ex vivo, in vitro, and in Silico Studies. *International Journal of Molecular Sciences*. **15** (3),
448 4795–822, doi: 10.3390/ijms15034795 (2014).
449 7. Patel, V.I., Metcalf, J.P. Airway macrophage and dendritic cell subsets in the resting
450 human lung. *Critical Reviews in Immunology*. **38** (4), 303–331, doi:
451 10.1615/CritRevImmunol.2018026459 (2018).
452 8. Bogorodskiy, A.O. *et al.* Murine Intraepithelial Dendritic Cells Interact With Phagocytic
453 Cells During Aspergillus fumigatus-Induced Inflammation. *Frontiers in Immunology*. **11**, doi:
454 10.3389/fimmu.2020.00298 (2020).
455 9. Kwon-Chung, K.J., Sugui, J.A. Aspergillus fumigatus-What Makes the Species a Ubiquitous
456 Human Fungal Pathogen? *PLoS Pathogens*. **9** (12), 1–4, doi: 10.1371/journal.ppat.1003743
457 (2013).
458 10. Overton, N., Gago, S., Bowyer, P. Immunogenetics of chronic and allergic aspergillosis.
459 *Immunogenetics of Fungal Diseases*. 153–171, doi: 10.1007/978-3-319-50842-9_7 (2017).
460 11. Thiesse, J. *et al.* Lung structure phenotype variation in inbred mouse strains revealed
461 through in vivo micro-CT imaging. *Journal of Applied Physiology*. **109** (6), 1960–1968, doi:
462 10.1152/japplphysiol.01322.2009 (2010).
463 12. Tochigi, N. *et al.* Histopathological implications of Aspergillus infection in lung. *Mediators*
464 *of Inflammation*. **2013**, doi: 10.1155/2013/809798 (2013).
465 13. Bruns, S. *et al.* Production of extracellular traps against aspergillus fumigatus in vitro and
466 in infected lung tissue is dependent on invading neutrophils and influenced by hydrophobin roda.
467 *PLoS Pathogens*. **6** (4), 1–18, doi: 10.1371/journal.ppat.1000873 (2010).
468 14. Shevchenko, M.A. *et al.* Aspergillus fumigatus Infection-Induced Neutrophil Recruitment
469 and Location in the Conducting Airway of Immunocompetent, Neutropenic, and
470 Immunosuppressed Mice. *Journal of Immunology Research*. **2018**, doi: 10.1155/2018/5379085
471 (2018).
472 15. Scott, G.D., Blum, E.D., Fryer, A.D., Jacoby, D.B. Tissue optical clearing, three-dimensional
473 imaging, and computer morphometry in whole mouse lungs and human airways. *American*
474 *Journal of Respiratory Cell and Molecular Biology*. **1** (51), 43–55, doi: 10.1165/rcmb.2013-0284OC
475 (2014).
476 16. Amich, J. *et al.* Three-dimensional light sheet fluorescence microscopy of lungs to dissect
477 local host immune-aspergillus fumigatus interactions. *mBio*. **11** (1), doi: 10.1128/mBio.02752-19
478 (2020).
479 17. Schindelin J, *et al.* Fiji: an open-source platform for biological-image analysis. *Nat*
480 *Methods.* **9** (7), 676–82. doi: 10.1038/nmeth.2019 (2012).
481 18. Li W, Germain RN, Gerner MY. High-dimensional cell-level analysis of tissues with Ce3D

multiplex volume imaging. Nat Protoc. **14** (6), 1708-1733. doi: 10.1038/s41596-019-0156-4 (2019).
19. Ertürk A, Lafkas D, Chalouni C. Imaging cleared intact biological systems at a cellular level by 3DISCO. J Vis Exp. (89), 51382. doi:10.3791/51382 (2014).
20. Kuhn, C. Biotin stores in rodent lungs: Localization to clara and type II alveolar cells. *Experimental Lung Research*. **14** (4), 527–536, doi: 10.3109/01902148809087825 (1988).

Figure



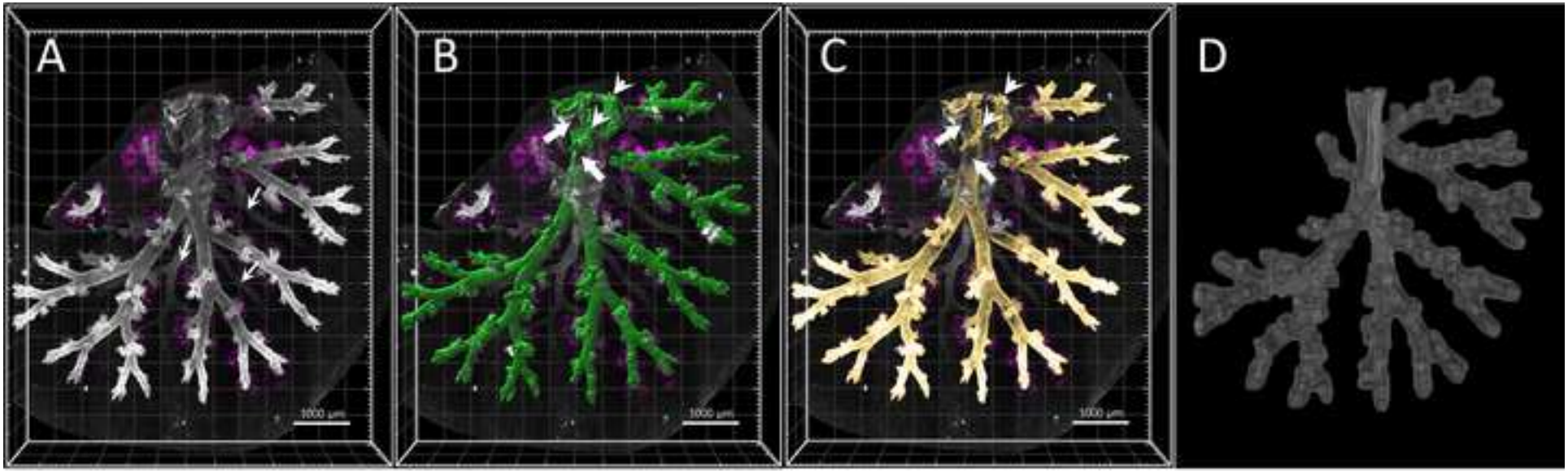

Figure



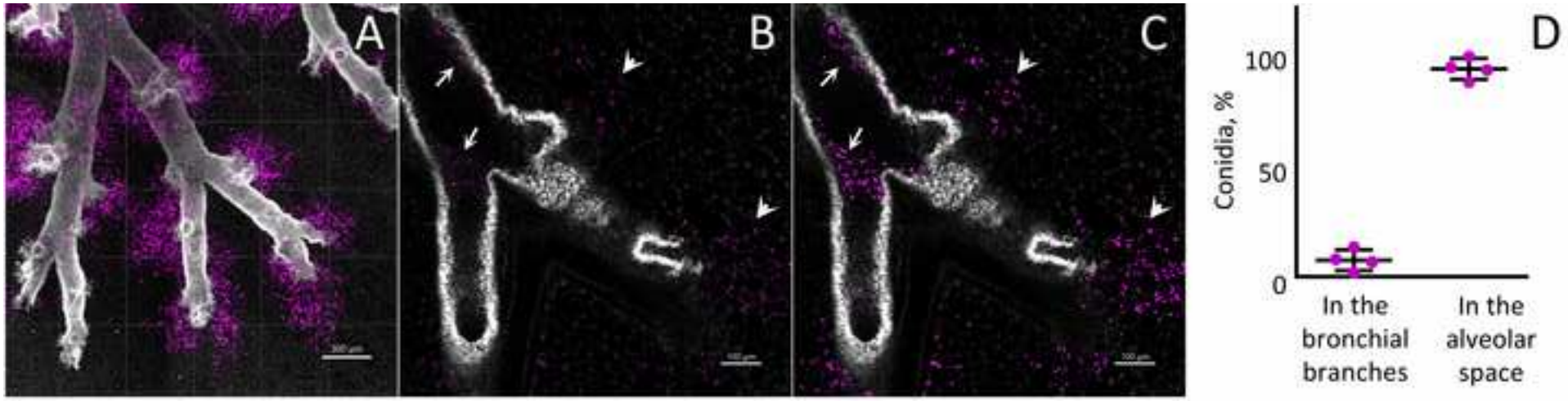

Dear Dr. Nam Nguyen,

We have increased the audio level and depleted the audio level peak exceeded -9 dB that we found between 14:09 and 14:19.

Thank you,

Marina Shevchenko